AGU100 ADVANCING EARTH AND SPACE SCIENCE

JGR

Journal of Geophysical Research: Atmospheres

RESEARCH ARTICLE
10.1029/2018JD028337

Key Points:
- A sequence of 10 X-ray pulses was observed from an aircraft inside thundercloud at 12-km altitude
- The pulses contain strong enhancement of the positron annihilation line (511 keV)
- Each pulse lasts for 1 s and is accompanied by a static discharge from the aircraft

Supporting Information:
- Supporting Information S1
- Data Set S1
- Data Set S2

Correspondence to:
P. Kochkin,
Pavlo.Kochkin@uib.no

Citation:
Kochkin, P., Sarria, D., Skeie, C., van Deursen, A. P. J., de Boer, A. I., Bardet, M., et al. (2018). In-flight observation of positron annihilation by ILDAS. *Journal of Geophysical Research: Atmospheres*, *123*, 8074–8090. https://doi.org/10.1029/2018JD028337

Received 16 JAN 2018
Accepted 14 JUN 2018
Accepted article online 23 JUN 2018
Published online 3 AUG 2018

In-Flight Observation of Positron Annihilation by ILDAS

P. Kochkin[1], D. Sarria[1], C. Skeie[1], A. P. J. van Deursen[2], A. I. de Boer[3], M. Bardet[3], C. Allasia[4], F. Flourens[4], and N. Østgaard[1]

[1]BCSS, University of Bergen, Bergen, Norway, [2]Electrical Engineering Department, Eindhoven University of Technology, Eindhoven, Netherlands, [3]The Netherlands Aerospace Centre, Amsterdam, Netherlands, [4]Airbus, Toulouse, France

Abstract We report a 511-keV photon flux enhancement that was observed inside a thundercloud and is a result of positron annihilation. The observation was made with the In-flight Lightning Damage Assessment System (ILDAS) on board of an A340 test aircraft. The aircraft was intentionally flying through a thunderstorm at 12-km altitude over Northern Australia in January 2016. Two gamma ray detectors showed a significant count rate increase synchronously with fast electromagnetic field variations registered by an on-board antenna. A sequence of 10 gamma ray enhancements was detected, each lasted for about 1 s. Their spectrum mainly consists of 511-keV photons and their Compton component. The local electric activity during the emission was identified as a series of static discharges of the aircraft. A full-scale Geant4 model of the aircraft was created to estimate the emission area. Monte Carlo simulation indicated that the positrons annihilated in direct vicinity or in the aircraft body.

1. Introduction

The first and the only report known to us on positron clouds inside thunderstorms was published in 2015 (Dwyer et al., 2015). The Airborne Detector for Energetic Lightning Emission flew on a Gulfstream V jet aircraft through the top of an active thundercloud in 2009. It contained two similar sensor assemblies vertically aligned and separated by 0.6 cm of lead. Each sensor consists of two 12.7-cm long 12.7-cm diameter BC-408 plastic cylinders, one NaI crystal of the same dimensions, and one small 2.54 × 2.54 cm^2 plastic scintillation detector intended to monitor high fluxes. At a certain moment during the flight the detectors showed a count rate increase. After analysis it was concluded that the increase mainly consisted of 511-keV photons. Photons of this energy are well defined and are a unique characteristic for positron annihilation process. The 511-keV emission lasted for at least 200 ms and was accompanied with pulses recorded by an electric field antenna. The pulses were assumed to be created by direct discharges on the antenna. Remarkably, no significant fluxes of particles with energy higher than the pair production threshold 1.022 MeV were detected sufficiently to explain the positron emission by this mechanism. Modeling indicated that the emission originated from a disperse cloud of positrons of 2-km radius. Different generation mechanisms were considered in the paper, and none of them was conclusive. Positron generation mechanism in thunderclouds remains a complete mystery and undoubtedly needs more in situ observations.

Lightning is known to generate microsecond-fast bursts of X-ray radiation (Dwyer et al., 2003; 2004, Dwyer, Rassoul, Al-Dayeh, et al., 2005; Dwyer et al., 2011; Hill, 2012; Hill et al., 2012; Howard et al., 2010, 2008; Mallick et al., 2012; Montanyà et al., 2012; Moore et al., 2001; Saleh et al., 2009; Schaal et al., 2014, 2013, 2012; Yoshida et al., 2008) and electron flux enhancements (Yoshida et al., 2008). Such bursts were detected from both natural and triggered lightning. The energy spectrum is typically in the few hundreds of keV range, exponentially decreasing without any specific lines. Lightning is seemingly also responsible for generation or triggering of Terrestrial Gamma Ray Flashes (TGFs) with energies up to several tens of MeV (Briggs et al., 2010; Connaughton et al., 2010, 2013; Cummer et al., 2011, 2005; Dwyer & Smith, 2005; Dwyer, Schaal, et al., 2012; Fishman et al., 1994; Gjesteland et al., 2017, 2011, 2012, 2010; Grefenstette et al., 2008; Hare et al., 2016; Marisaldi, Argan, et al., 2010; Marisaldi, Fuschino, et al., 2010; Marisaldi et al., 2014; Mezentsev et al., 2017; Østgaard et al., 2013, 2012, 2008; Smith et al., 2005, 2011a, 2011b), or maybe higher (Tavani et al., 2011). Typical TGF duration varies from tens to several hundreds of microseconds. On smaller scales meter-long laboratory discharges are also able to generate X-ray bursts of nanosecond duration (Babich & Loiko, 2009; Carlson et al., 2015; Dwyer, Rassoul, Saleh, et al., 2005; Dwyer et al., 2008; Kochkin, 2014; Kochkin et al., 2012, 2014a, 2014b;

Kochkin, Köhn, et al., 2016; Kochkin, Lehtinen, et al., 2016; March & Montanyà, 2010, 2011; March et al., 2012; Nguyen et al., 2008, 2009; Østgaard et al., 2016; Rahman et al., 2008; Rep'ev et al., 2008). The bursts were first suggested to be generated in streamer encounters (Cooray et al., 2009), but encounters alone are apparently not a sufficient condition (Babich & Bochkov, 2017; Ihaddadene & Celestin, 2015; Köhn et al., 2017). And finally, microsecond-fast bursts of gamma radiation inside aircraft were reported in association with recoil processes in lightning discharges (Kochkin et al., 2015).

Apart from these transient phenomena, long-lasting gamma ray glows of thunderclouds were reported in association with strong electric fields (Eack et al., 1996a, 1996b, 2000; Kelley et al., 2015; Kochkin et al., 2017; McCarthy & Parks, 1985; Parks et al., 1981). They last from seconds to hundreds of seconds, maybe even longer. The glows were also observed from ground (Brunetti et al., 2000; Chubenko et al., 2000; Torii et al., 2002, 2009; Tsuchiya et al., 2007) and often accompanied by neutrons (Chilingarian et al., 2012, 2010; Gurevich et al., 2012; Kuroda et al., 2016; Tsuchiya et al., 2012) and electron fluxes (Chilingarian, Vanyan, & Mailyan, 2013). Their gamma ray spectra can be consistent with the Relativistic Runaway Electron Avalanche (RREA) mechanism (Babich et al., 2010; Tsuchiya et al., 2007) first introduced in Gurevich et al. (1992). Alternative models for gamma ray flux enhancement can be found in Chilingarian, Hovsepyan, and Kozliner (2013) and McCarthy and Parks (1992). A review of the currently known atmospheric phenomena and physical mechanisms behind them can be found in Dwyer, Smith, and Cummer (2012).

Another new type of indirect TGF observations quickly attracts scientific attention. TGFs should seemingly create a long-lasting neutron emission, with associated isotope production. Such emission was observed from the ground (Bowers et al., 2017; Teruaki et al., 2017), though the TGF was not clearly detected, maybe because of the limited count rate capability of the detectors. A similar phenomenon was modeled at higher altitudes (Babich, 2006) and called a *TGF afterglow* (Rutjes et al., 2017). Neutrons in such afterglow are supposedly created in photonuclear reaction and can remain detectable on a subsecond scale for at least downward directed TGFs. The isotopes created from these photonuclear reactions are β^+ emitters that can produce a 511-keV line enhancement in the observed spectrum than can last for tens of seconds.

In this manuscript we report the observation of a particle emission in similar conditions as in Dwyer et al. (2015). The aircraft intentionally flew through an active thunderstorm at 12-km altitude in Northern Australia. Periodic electric field pulses were detected by the electric field antenna. Analysis of the recorded data allowed to classify the pulses and their origin. The pulses were correlated with a second-long gamma ray emission. The spectrum of the emission contains a prominent 511-keV line. Simultaneously, an on-board video camera captured an optical phenomenon originated from the left wing of the aircraft. This is the first time when positron annihilation has been detected synchronously with optical observations. A detailed full-scale Geant4 model of the aircraft was created. The model incorporates the gamma ray detectors, the aircraft, and most of the massive equipment around them. It was used to estimate the size of the positron annihilation area.

2. Instrumentation

In-flight Lightning Damage Assessment System (ILDAS) is the airborne platform dedicated to flying *through* thunderstorms and investigate lightning interaction with aircraft in situ. It was initially designed to measure lightning current waveform and derive characteristics such as current entry and exit points, amplitude, and to assess the possible structural damage to the aircraft. The system was later extended with two gamma ray detectors. The extension allowed us to obtain unique measurements of gamma radiation inside the aircraft synchronously with the lightning waveforms. The detectors are 4-cm-diameter 4-cm-long $LaBr_3$ cylinders attached to a photomultiplier tube in a sealed aluminum casing. Besides the detectors, the system contains one electric field (E-field) sensor, and eight magnetic field (H-field) window sensors. The E-field sensor is a flat plate antenna attached to the fuselage window from inside in the forward fuselage. It measures the *local* electric field (not dE/dt) near the aircraft body, which should not be confused with the ambient electric field in the cloud. The local field around sharp objects can be higher than ambient due to electrostatic induction. The H-field window sensors are designed to determine the current direction through the aircraft and measure the current sheet density in A/m. They are located at different positions along the fuselage. Photographs of the sensors and gamma ray detectors can be found in Kochkin et al. (2015) Figures 2 and 3. Both E- and H-field sensors are differentiating, and subsequent analog integration provides a flat response over the frequency

band from 100 Hz to 10 MHz for H-field and 10 Hz to 500 kHz for E-field. The sampling rate for both sensors is 83.3 MS·s^{-1}, which corresponds to 12-ns resolution time. The gamma ray detectors are sampled with 10-ns resolution.

The system provides two data acquisition methods: continuous and triggered. Continuous acquisition provides E- and H-field maximum, minimum, and average values in 17-ms time intervals for each individual sensor. Pulses from photomultiplier are counted in six different individual energy channels for each gamma ray detector in 15-ms time window. The total number of pulses summed over all channels will be considered in this paper. Only gamma rays with energy greater than 100 keV are counted. Triggered acquisition provides data at the full sampling rate for a limited duration of 1.0 to 1.2 s. The trigger condition for the system is based on real-time analysis of the E- and H-field sensor data. When a characteristic discharge signature is identified, the system stores the measurement data from all sensors, including the gamma ray sensors. E- and H-field data are stored with a 12-ns sampling interval for 1.2 s, while gamma ray data are stored with a 10-ns sampling interval for 1.0 s. More details about ILDAS and its design can be found in Zwemmer et al. (2009), de Boer et al. (2011, 2013, 2015), Stelmashuk et al. (2008, 2007), van Deursen and Stelmashuk (2011), and van Deursen (2011).

There were nine video cameras in the frame of another research project on board the same aircraft with ILDAS. The cameras were located inside the aircraft and pointed toward wings, ice accretion probes, cockpit windshield, and instrument panel. The cameras were operating at 25 frames per second rate continuously and allowed to monitor discharge activity near the aircraft during the entire flight.

To locate lightning strikes, data from two ground-based lightning location networks were used. One is the global World Wide Lightning Location Network (WWLLN), the second is the local Australian network called the Lightning Incident Archive Search (LIAS). It is a commercial network which is operated by The Global Position and Tracking Systems Pty. Ltd. WWLLN location accuracy is estimated as 5-km radius over the region of observation (Rodger et al., 2004). LIAS network has better accuracy with 250- to 500-m uncertainty. It reports more sferics and provides additional data regarding event type, polarity, and peak current. While WWLLN is mainly sensitive to cloud-to-ground lightning, LIAS can also detect intracloud discharges. WWLLN data were available for this study on large scale than LIAS.

The data from HIMAWARI-8 satellite (HIMAWARI-8, 2017) were used to reconstruct cloud top hight (CTH) profile during the flight. Reflectivity maps of the region of interest were obtained in infrared 11-μm range.

3. Observation

On 14 January 2016 an Airbus A340-600 factory test aircraft intentionally flew through a thunderstorm in Northern Australia. Its starting base was at Darwin International Airport. Figure 1 shows the flight track and the gamma ray count rate inside the aircraft. Top panel shows the zoomed in map on the aircraft path containing the most interesting observations. Bottom panel shows the gamma ray count rate binned in 15 ms from 07:15:00 to 08:00:00 UTC. Running average with 1-s window was applied to reduce the noise. LIAS sferics detected during this time period are plotted on the top panel as gray dots. Only sferics within 50-km radius from location A were available. Middle panel shows the altitude profile. The aircraft was flying from 11.2 to 12.5 km during this period. Three peaks can be identified on the plot, they are labeled from A to C. The gamma ray count rate increase that happened before A, from 07:16:00 to 07:19:00, is partly caused by the altitude change. In addition to the altitude effect, a gamma ray glow is also present at the moment A. The count rate increases at B and C are also attributed to long-duration gamma ray glows. It is very important to have correct altitude measurements and background count rates for any analysis. In our case, only background is measured between A, B, and C.

The brief gamma ray pulses at A during the glow are the main object for investigation in this paper and will be considered in greater detail below. Fifteen minutes after them, at 07:34:00 when the aircraft was at location B, another gamma ray glow was detected. It was not accompanied by high electrical activity and was not terminated by a lightning flash during the observation. ILDAS was not triggered during event B. The particle count rate almost doubled at the peak of the glow with respect to background. And finally, 20 min after the glow, at 07:54:00, when the aircraft was at location C, another enhancement of gamma ray count rate was observed. It resembles the phenomenon detected in location A but has much less number of counts for analysis.

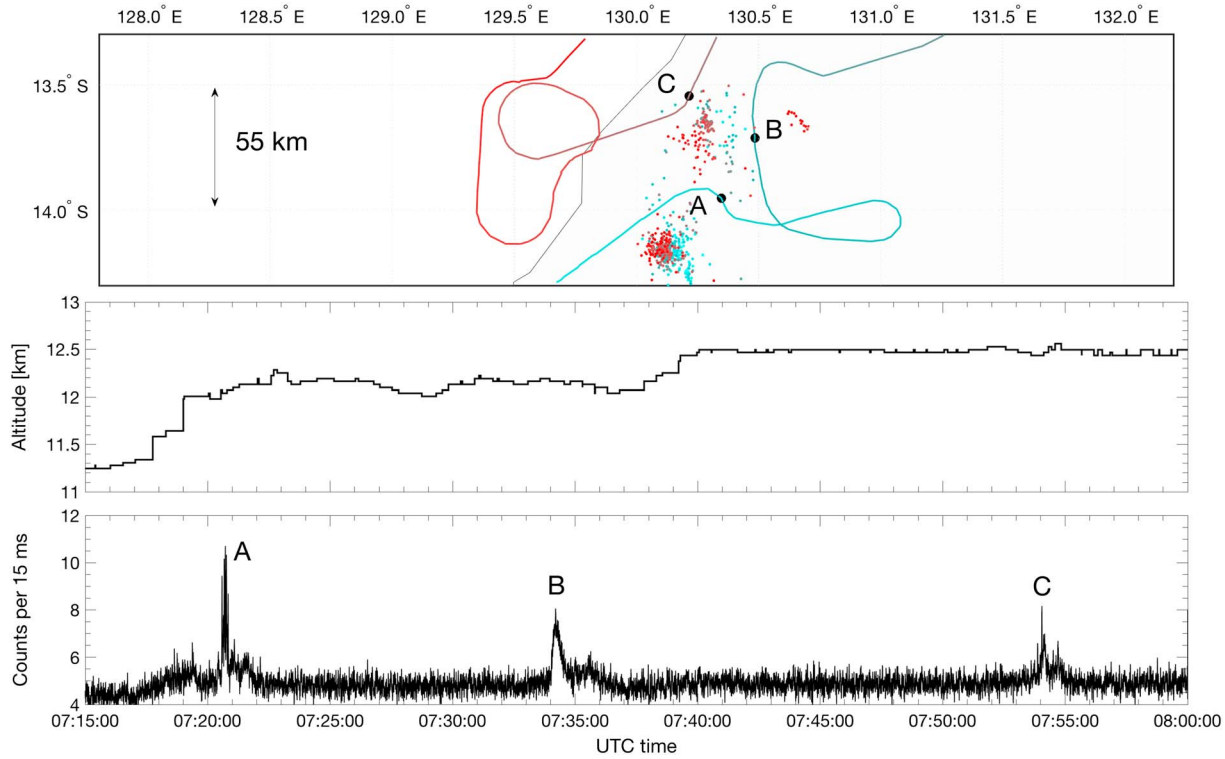

Figure 1. The flight path and the gamma radiation inside the aircraft. The top panel shows the color-coded path of the aircraft from earliest at 07:00:00 (blue) to latest at 08:30:00 (red). Three specific locations are marked from A to C. Lightning Incident Archive Search sferics from 07:15:00 to 08:00:00 UTC are plotted and also color coded from earliest (blue) to latest (red). The middle panel shows the altitude profile. The bottom panel shows the total gamma ray counts per 15 ms during this period. A running average smoothing algorithm with 1-s window is applied to reduce the noise.

On bigger scale, Figure 2 shows the flight track as plotted on a temperature map. The three locations A, B, and C are indicated. The map was obtained 10 min after the moment when the aircraft was at location A, at 07:30:00 UTC. By comparing the cloud top temperature from the map with the reconstructed troposphere vertical profile as predicted by the European Center Medium Weather Forecast, the CTH can be estimated. In our case, the CTH was higher than 15 km for the regions with temperature below −70°. WWLLN lightning sferics are plotted from moment A to C. During this period the aircraft speed was 230 m/s.

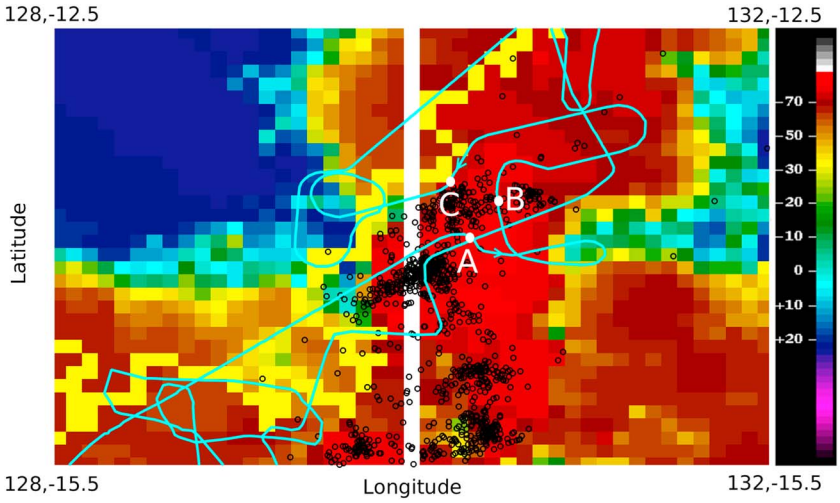

Figure 2. The infrared HIMAWARI-8 satellite image. Temperature scale is indicated on the right side in degree Celsius. The red regions with t≤ − 70° correspond to the Cloud Top Height ≥ 15 km. World Wide Lightning Location Network sferics are shown from moment A to C as black circles.

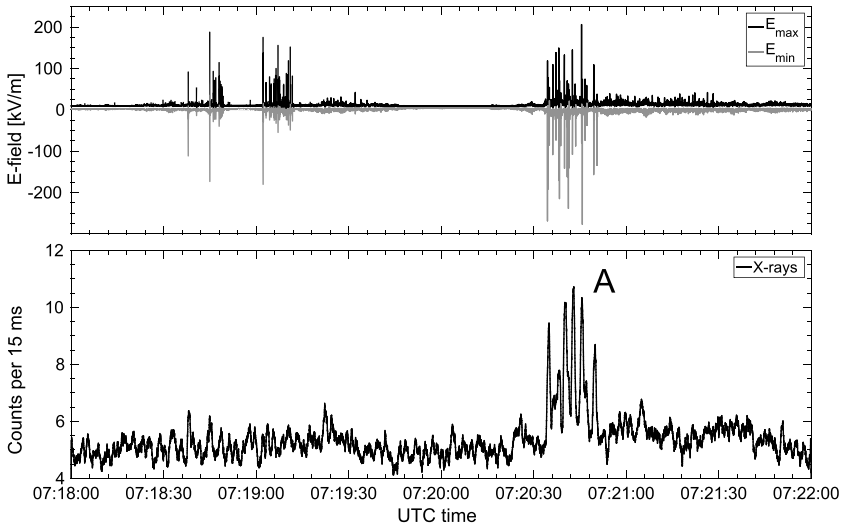

Figure 3. The electrical activity and gamma ray count rate during 4 min of flight near location A. The photon counts are binned in 15 ms and smoothed with 1-s running average. The aircraft moved 57 km during this period with speed 236 m/s (459 kts). Gamma ray enhancement was not observed during the first sequence of E-field pulses from 07:18:30 to 07:19:30, but remarkable count rate increase is evident during the second sequence from 07:20:30 to 07:21:00.

Figure 3 shows the local E-field measurements and gamma ray count rate during 4 min near location A. This corresponds to 57-km traveled distance with speed 236 m/s (459 kts). E-field is plotted as maximum E_{max} and minimum E_{min} values on 17-ms interval. The first group of E-field pulses starting from 07:18:30 to 07:19:30 are not associated with any photon count rate increase. In contrast, the second group of pulses from 07:20:30 to 07:21:00 is clearly accompanied with periodic gamma ray enhancements. The ILDAS system triggered four times during the plotted period. Below we consider each of these triggers individually.

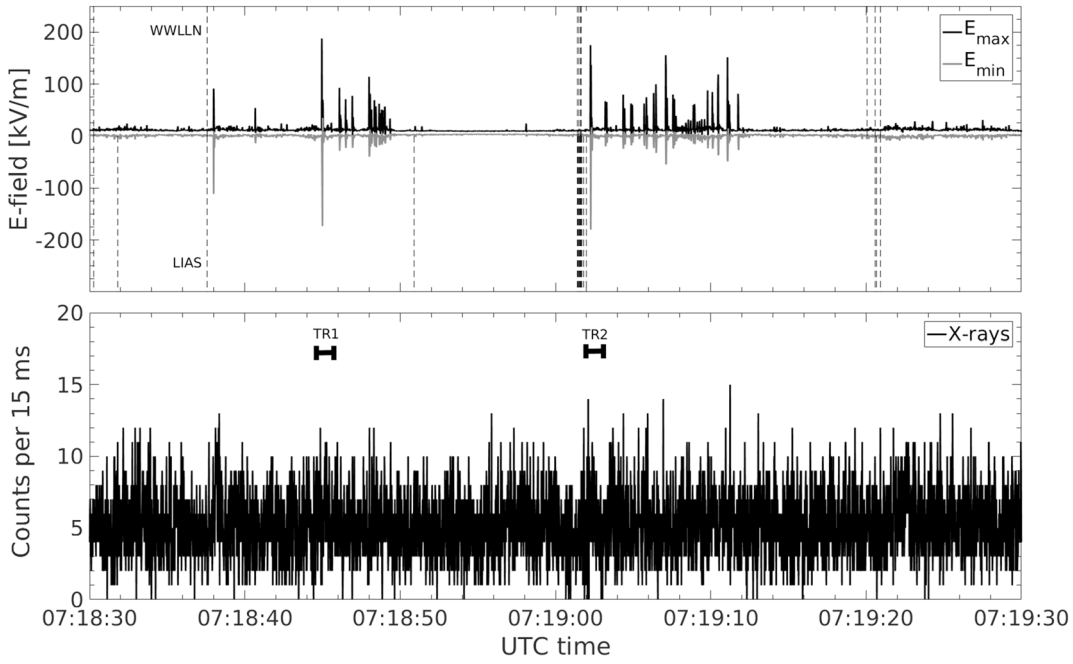

Figure 4. Zoom in of the first group of E-field pulses plotted in Figure 3. Electric field is plotted as maximum and minimum values in 17-ms intervals. Photon counts from both detectors are binned in 15-ms intervals and plotted without smoothing. Only gamma rays with energy greater than 100 keV are counted. World Wide Lightning Location Network (WWLLN) and Lightning Incident Archive Search (LIAS) sferic times are plotted as vertical dashed lines.

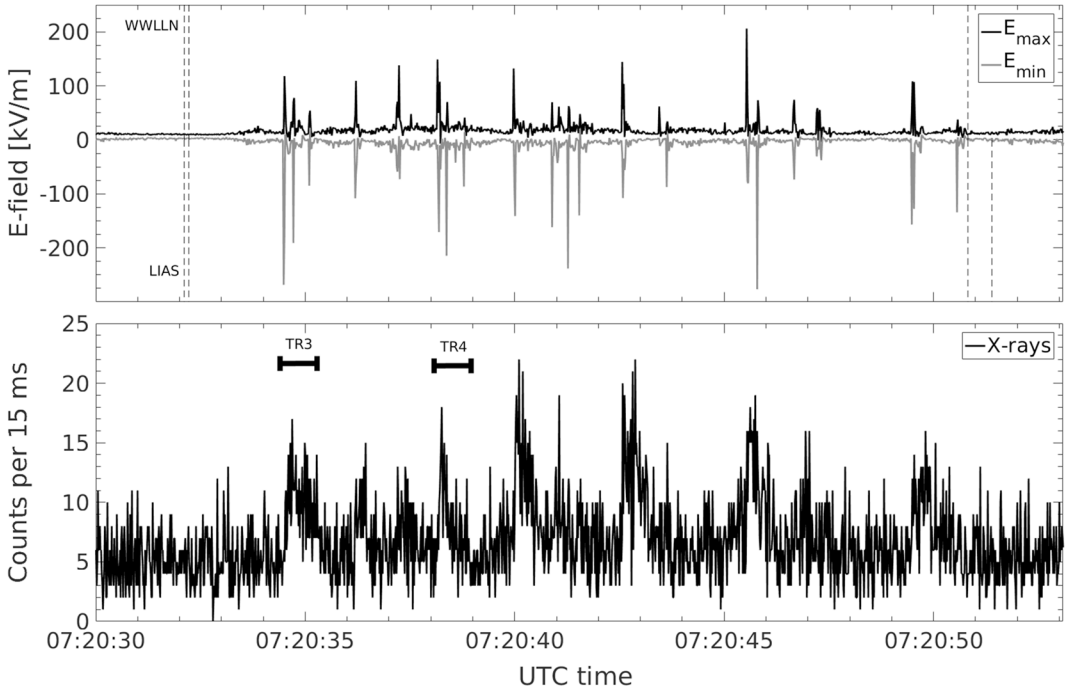

Figure 5. Zoom in of the E-field pulses at the moment A. Gamma ray pulses from both detectors are counted in 15 ms time bins. Only original Continuous Data File (CDF) data are plotted without smoothing. Up to 10 pulses are visible, and each lasts for roughly 1 s. They all are associated with fast E-field changes. In-flight Lightning Damage Assessment System double system was triggered two times and recorded triggers TR3 and TR4 with high resolution. World Wide Lightning Location Network (WWLLN) and Lightning Incident Archive Search (LIAS) sferics do not correlate with the E-field changes.

Figure 4 shows zoomed in plot on the first group of the E-field pulses. ILDAS recorded two subsequent triggers TR1 and TR2. They are indicated as horizontal segments of 1.2-s duration. Both triggers can be conditionally classified as aircraft-triggered discharges (Lalande et al., 1999; Laroche et al., 2012; Mazur et al., 1984; Mazur & Ruhnke, 1993; Moreau et al., 1992). Conditionally because their characteristic E-field pattern still resembles an aircraft-triggered discharge but develops much faster than previously observed at lower altitudes (Kochkin et al., 2015). The aircraft-triggered discharge, in contrast to the aircraft intercepted, starts with initiation of a leader from an aircraft extremity. Shortly after, another leader of opposite polarity initiates from the opposite extremity. This happens when the aircraft is exposed to a strong ambient electric field. Two leaders propagate in opposite directions, which leads to the formation of a lightning flash with high-current (tens of kiloamperes) recoil pulses. Triggers TR1 and TR2 are likely positive static discharges in the presence of significant ambient electric field. Static discharges are periodic/pulsating discharges with relatively low current (tens to hundreds of amperes). They usually do not develop into a lightning flash. The times of WWLLN and LIAS sferics are indicated as vertical dashed lines. There is no obvious association between the lightning sferics and the E-field pulses measured by ILDAS. Time interval between the last sferic and the first E-field pulse was at least 250 ms. In addition, lightning activity right before TR2 was behind the aircraft 30 km away from the trajectory to the right. As was demonstrated in Kochkin et al. (2017), ILDAS is capable to detect distant flashes with 17-ms uncertainty.

Figure 5 shows the E-field and gamma ray measurements at the moment A. Around 10 gamma ray enhancements in association with fast E-field changes can be seen on the plot. ILDAS was again triggered two times and stored high-resolution data for triggers TR3 and TR4. Trigger intervals are indicated on the plot. Two gradually decaying photon enhancements were recorded with the highest possible 10-ns resolution. Photon counts from both detectors are binned in 15-ms intervals and plotted without running average, background subtraction, or any other processing. Only photons with energy greater than 100 keV are counted. The maximal single photon energy that was detected during this campaign is 10 MeV. The largest gamma ray enhancements lasted for almost 1 s. The emissions decay with a half-life close to 200 ms. WWLLN and LIAS

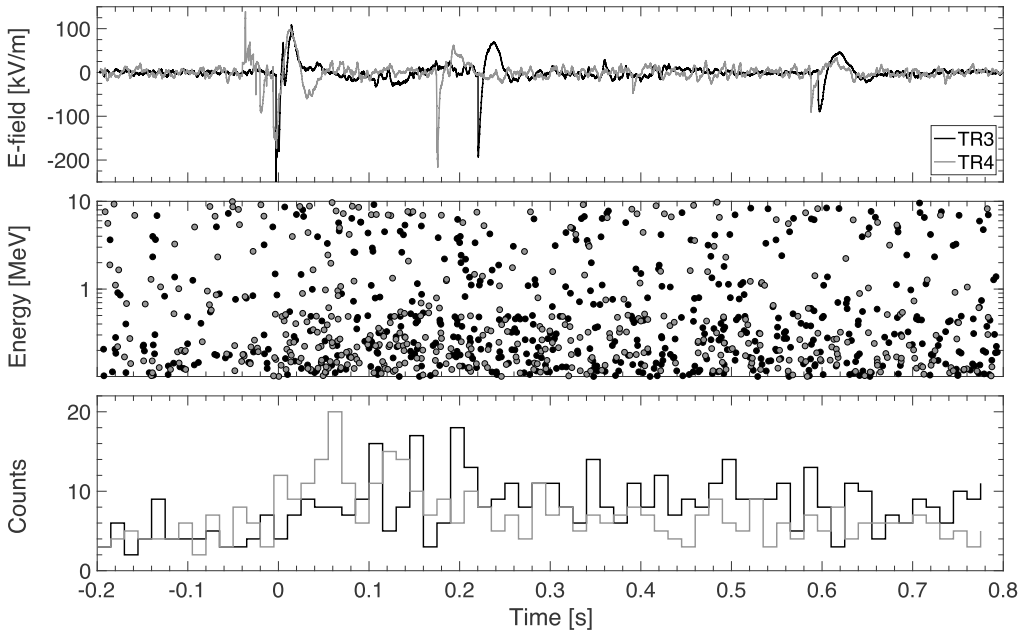

Figure 6. Both triggers TR3 (black) and T4 (gray) are plotted together. Top panel shows E-field data. Middle panel shows photons from 0.1 to 10 MeV on logarithmic scale. Bottom panel shows photon counts from 0.1 to 10 MeV in 15-ms bins.

sferics were 20–40 km away behind the aircraft. The time interval between them and the E-field pulses was more than 2 s.

The high-resolution data from two triggers TR3 (black) and TR4 (gray) are plotted in Figure 6. Top panel shows the signal from E-field antenna. Fast-changing E-field pulses are seen, surprisingly similar in both triggers. Middle panel shows the scattered plot where each dot corresponds to a single photon. All photons detected by two detectors with energy greater than 100 keV are plotted. Neither pile-up nor multiphoton bursts were found in the data after the analysis of each individual photomultiplier tube pulse and comparison with single photon pulses measured in the laboratory. Not even an Extensive Air Shower that would lead to a simultaneously recorded signal by two detectors was identified. Bottom panel shows the photons binned in 15 ms. A gradual count rate increase is seen that starts after the first E-field pulse at $t = 0$.

First remarkable observation is the periodic pulsation of the E-field signal. As can be seen for the top panel, both triggers consist of electromagnetic pulses of similar shape and magnitude. The pulses appear with ~200-ms intervals. Trigger TR3 (black line) contains three such pulses at 0, 200, and 600 ms, while trigger T4 (gray) registered four pulses at 0, 200, 400 (small), and 600 ms. These pulses can also be seen in low-resolution data in Figure 5 during the indicated trigger intervals. Similar periodic pulsation was observed after the gamma ray glow termination in Kochkin et al. (2017).

Second, it is clear from Figures 3 and 5 that these periodic E-field pulses are closely associated with gamma ray emission. However, the association becomes less obvious when plotted on a finer time scale, such as in Figure 6. There are no microsecond-fast photon bursts during the emission; each of the photon signals can be fitted to a single-photon response function of the detector. In fact, the count rate increase has a longer duration than the E-field variation. In addition, they do not strictly correlate in time. After the first E-field pulse at time zero the gamma ray emission gradually increases and reaches its maximum after 50–200 ms. Subsequent E-field pulses have less such effect, if any. This figure clearly demonstrates that the E-field pulse happened before the photon enhancement. This does not, however, imply direct causality.

3.1. Electrostatic Discharges

Static dischargers, or static wicks, are the devices with high electrical resistance but low voltage threshold for corona initiation. They are installed on the trailing edges of the aircraft and are intended to control the aircraft discharging into the surrounding atmosphere. The aircraft accumulates charge from charged cloud particles directly or by friction with air in phenomenon known as triboelectric charging or precipitation static.

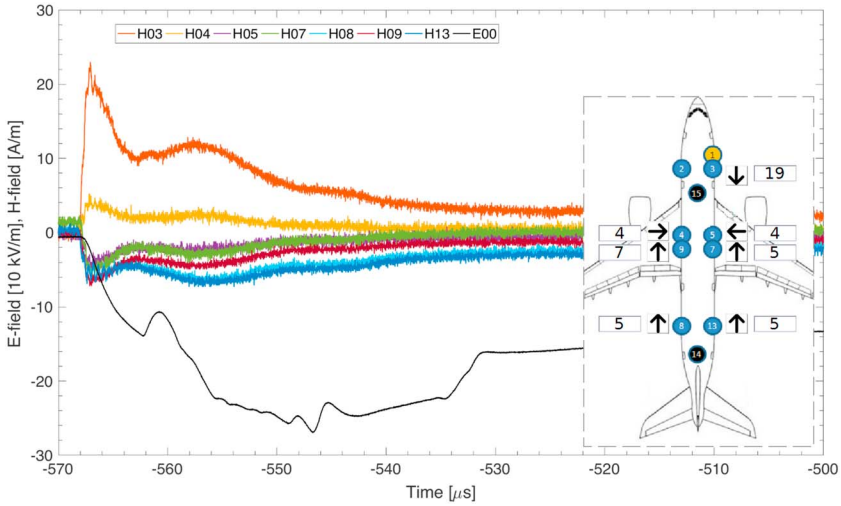

Figure 7. The In-flight Lightning Damage Assessment System sensor recordings at the moment of the first pulse of TR3. The inset shows the current direction (arrows) and the surface current density (values in A/m) through each window sensor. The H-field sensors are the blue circles. The E-field sensor is the yellow circle located in the forward fuselage. The current and E-field patterns indicate that electrons were emitted out of the aircraft in all directions. The E-field sensor has 10 kV/m units for better visualization on the plot.

By dumping small controlled portions of charge out from the aircraft, the dischargers reduce the chance to trigger a lightning strike. It will be shown below that the E-field pulses in Figure 5 are consistent with this process.

It is well known that flying through high-level clouds can generate *P-static* (P for precipitation). When aircraft fly through clouds, they usually accumulate negative charge on their outer surface (Illingworth & Marsh, 1986). The total charging current I_{ch} depends on many parameters such as ambient conditions, particle size and shape, aircraft speed and material. In such conditions the aircraft potential V builds up as

$$\frac{dV}{dt} = \frac{I_{ch} - I_{dis}(V)}{C} \quad (1)$$

where C is the aircraft capacitance, I_{ch} and I_{dis} are the total charging and discharging currents. Assuming the aircraft capacitance roughly $C = 1$ nF (Tanner & Nanevicz, 1961) and charging current somewhat below $I_{ch} = 1$ mA the potential will increase with 1 MV/s maximal rate. This process will continue until the local electric field near the aircraft extremities reaches a certain threshold value. The discharge current, I_{dis}, is assumed to be zero before crossing this threshold. Streamer corona can start forming at 100–300 kV/m field strength at 12-km altitude. Due to the field enhancement on the extremities, even small charges on the aircraft can initiate corona discharges. Therefore, the surface charge is practically limited to hundreds of μC, maximum aircraft potential to several hundreds kilovolts, and charging time to a fraction of a seconds. Let us consider these processes in more detail.

Figure 7 shows the ILDAS data at the moment of the first electromagnetic pulse of TR3. The H02 sensor is missing because of the instrument's limited buffer size and finite data transfer speed to the ILDAS on-board computer. The inset shows the current density amplitudes (in A/m) and directions at the peak time. Most of the current came from the nose. The electrons move against the current, hence out of the aircraft. But the discharge certainly never evolved into a lightning flash, as was many times observed by ILDAS in other occasions (Kochkin et al., 2015). The current pulse gradually falls down to zero until the next pulse comes after 200 ms. To obtain the average current through the aircraft body, one needs to multiply the current sheet density by a factor of $2\pi R \approx 20$, where R is the fuselage radius 2.8 m. According to the data, the electrons start to flow out of the aircraft, which leads to the local E-field reduction. Negative E-field change (dE/dt) can indicate, (i) accumulation of positive charge on the aircraft surface or (ii) removal of negative charge from the surface. The H-field sensors indicate that electrons were moving away from the aircraft in all directions. The E-field change is linearly proportional to the charge removed from the surface.

Charge accumulated on the surface and ambient electric field will be enhanced by the aircraft and both contribute to the local electric field. Thus, the electric field strength at the surface can be described as

$$E_s = \left(E_0 \cdot k_1 - \frac{Q}{\epsilon_0 A}\right) \cdot k_2 \tag{2}$$

where E_s is the local surface electric field, E_0 is the ambient electric field, k_1 is the enhancement coefficient related to geometric form of the aircraft body, k_2 is the additional multiplication factor introduced by sharp objects, ϵ_0 is the free space permittivity, A is the aircraft surface area that roughly equals to 1,500 m^2. The k_2 coefficient considered below is only valid for the local extremities under consideration and is in general different for different sharp protrusions of the aircraft. In constant ambient field the local electric field *change* is dictated by the static discharge and hence:

$$\Delta E_s = -\frac{\Delta Q}{\epsilon_0 A} \cdot k_2 \tag{3}$$

The E-field change caused by the discharge can be derived from the antenna measurements. Total charge removed in one pulse can be obtained by integrating the H-field signals. For example, the current pulse that is shown in Figure 7 removed $\Delta Q = 0.8$ mC or $10^{15}-10^{16}$ electrons. This value is underestimated because ILDAS does not measure charges sited on the wings. At the same moment the surface E-field decreased by $\Delta E = 250$ kV/m and overall aircraft potential is reduced by roughly $\Delta U = \Delta Q/C = 0.8$ MV. Substituting the observed E-field changes and the total removed charges to expression (3), the k_2 coefficient can be found $k_2 \approx 5$. The ambient electric field E_0 and the field created by the surface charge is enhanced by this factor.

In the absence of surface charge, the equation (2) simplifies to $E_s = E_0 \cdot k_1 k_2$. As discussed above, the surface electric field cannot exceed streamer corona threshold for long time. Thus, $E_0 \cdot k_1 k_2 \leqslant 100-300$ kV/m. Coefficient k_1 is defined by aircraft geometric shape and the actual ambient field configuration. The aircraft can be approximated by an ellipsoid with longitudinal and transverse to E-field lines components a and b. The k_1 depends on the ratio a/b and can be looked up in empirical tables for example in Muehleisen (1980). For the A340-600 aircraft k_1 only slightly exceeds 1 because its length and wingspan are almost even (75 and 63 m, respectively). Thus, *if* the ambient electric field exceeds $E_0 = 20-60$ kV/m the local surface field becomes high enough to initiate static discharges. This value is on the order of the RREA threshold at this altitude $E_{th} = 50$ kV/m. By the same reason, in the absence of local electric field the amount of charge that can be accumulated on the surface is limited. It roughly equals to $Q_{\max} \leqslant 0.2-0.6$ mC, very close to 0.8 mC that was removed by the static discharge considered above. Thus, apparently all surface charges are removed from the aircraft by the current pulse. This also implies that the local electric field was mostly created by the surface charge and the ambient electric field must be weak. In this case, the static discharges should follow the wingtip vortex channel core, instead of being guided by the field lines. Optical observation by video camera confirms this suggestion.

Remarkably, no photon flux enhancement was observed in association with the first two triggers TR1 and TR2. They start with a positive leader but quickly launch a negative leader from opposite side. The polarities were derived from the H-field measurements and the associated current density direction. They are likely positive static discharges developing in an ambient electric field. Identical current pattern scenarios were found in both triggers, despite the fact they are 18 s apart, enforcing the suggestion that they are static discharges. The analysis of the E-field pulses in all triggers TR1-TR4 allows us to conclude that they are caused by static discharges.

3.2. Optical Observation

Figure 8 shows faint sparks from static dischargers at the wingtip device. Color-adjusted inset unveils the second spark, which is not obvious on the original image. The video frame was taken at 07:20:38.80 UTC, synchronously with TR4. The discharge is clearly initiated at the discharger device and propagated along the vortex channel core of low pressure. This is certainly not an aircraft-intercepted lightning discharge. However, a more intense discharge could be formed from the nose since the largest current ran through it. The ambient electric field is apparently weak, because in high fields the discharge follows the field direction as was observed in Kochkin et al. (2017). However, most of the lightning activity is concentrated exactly on the left side and behind the aircraft at this moment (see Figure 2). So the ambient field can actually be pointed toward the left wing more or less aligned with the vortex core and may not alter the discharge direction. Direct ambient field measurements with field mils would help to understand the electric field dynamics better.

Figure 8. The image of the static discharge on the left wing. Color-adjacent inset is shown to enhance the visual perception. The discharge follows the vortex channel core of reduced pressure. The time is indicated in the left corner and corresponds to TR4.

Two more sparks have been detected at nearly this time. They are shown in Figure 9. Left image shows the same left wing as was discussed above. Right image shows an ice accretion probe attached from outside to the left side of the cockpit. The frames were taken at 07:20:43.20 and 07:20:46.24 UTC both synchronously with gamma ray enhancements but without ILDAS triggers. The enigmatic bright spot at the right image is present on entire video footage and not related to the discharge activity. It is likely a reflection in the cockpit glass. Besides these three sparks shown in Figures 8 and 9, cameras did not observe other optical phenomena during the gamma ray pulses. It does not mean, however, that discharges did not happen at this time. The cameras did not monitor the entire aircraft surface.

3.3. Gamma Ray Spectrum

The gamma ray spectra during the four ILDAS triggers are shown separately in Figure 10. Photons are binned in 80 logarithmic bins from 0.1 to 10 MeV. Top two panels correspond to the triggers without gamma ray enhancement TR1 and TR2. Bottom two are the triggers during which the gamma ray flux was increased. The TR3 spectrum has surprisingly bright 511-keV line. As can be seen from Figure 5, TR4 contains significantly shorter photon flux enhancement than TR3. It explains why its 511-keV line is not as bright as in TR3. Absorption efficiency for the used LaBr3 crystal decays from 100% to 50% in the plotted energy range (Rozsa et al., 2009).

There were total 338 and 300 gamma ray photons between 0.1 and 10 MeV detected during TR1 and TR2, respectively, which gives the average background count rate at this altitude 319 ± 27 photons per second. During TR3 and TR4 there were 559 and 452 photons detected. This gives 240 ± 27 and 133 ± 27 photons from the unknown emission source in TR3 and TR4. Considering only the 511-keV line, there were 5.5 ± 0.7 photons in the energy bin from 0.483 to 0.512 MeV during TR1 and TR2. During TR3 and TR4 there were 28 and 13 photons

Figure 9. The original camera images of the discharge activity from the aircraft. Left image shows the vortex channel re-brightening behind the left wing tip. Right image shows the probe for ice accretion measurement located on the cockpit left top. Both images contain discharges that happened synchronously with gamma ray enhancements.

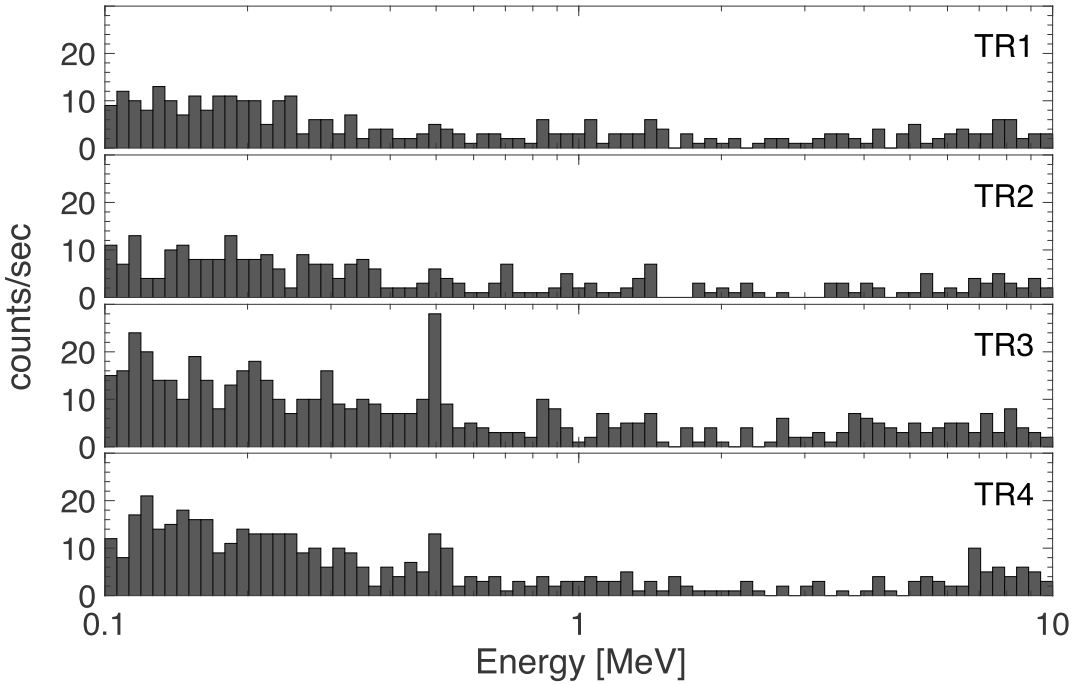

Figure 10. The histogram of the photon energies during the four ILDAS triggers (no background subtraction). TR1 and TR2 were recorded without gamma ray enhancement. In contrast, photon flux increased during TR3 and TR4. The prominent 511 keV line can be seen in TR3 histogram. Notice that bins are constant in log scale, which means larger bin size at higher energies.

detected in this energy range, respectively. In addition, there were 89 ± 17 potentially pair-producing photons with energies above 1.022 MeV in TR1 and TR2. During TR3 and TR4 the number of such photons increased to 140 and 102, respectively. Thus, more than 400% increase of 511-keV photons in TR3 was accompanied by only 50% increase of pair-producing photons. The numbers are summarized in Table 1.

It is clear that the observed phenomena involve positron annihilation. The key questions are where and how the positrons are produced. There are two reasonable ways to produce positrons, (i) pair production from gamma rays and (ii) isotopes undergoing β^+ decay. The second option is interesting, taking into account recent observations of Teruaki et al. (2017) and Bowers et al. (2017). However, it has a conceptual problem with the energy source and will be left to a future study. In section 4, we briefly examine the feasibility of pair production. To investigate the nature of the observed phenomenon, a Geant4 model of the aircraft and the detectors was created. The model was used in various Monte Carlo simulations to estimate the annihilation area and the response to a hypothetical photon burst produced by a runaway electron avalanche. The model description can be found in Appendix A.

4. Simulation Results

In this section, we compare simulated spectra against the measured background subtracted spectrum. The last was obtained by subtracting counts of TR2 from counts of TR3. Error bars were estimated according to uncertainty propagation $\sigma^2_{\text{total}} = \sigma^2_{\text{TR2}} + \sigma^2_{\text{TR3}}$, where σ_{total} is the uncertainty of the background subtracted spectrum, σ_{TR2} and σ_{TR3} are the standard deviations of TR2 and TR3, respectively.

Table 1
The Number of Gamma Ray Photons Detected in the Energy Range

Energy range (MeV)	TR1	TR2	TR3	TR4
0.1–10	338	300	559	452
0.483–0.512	5	6	28	13
1.022–10	101	77	140	102

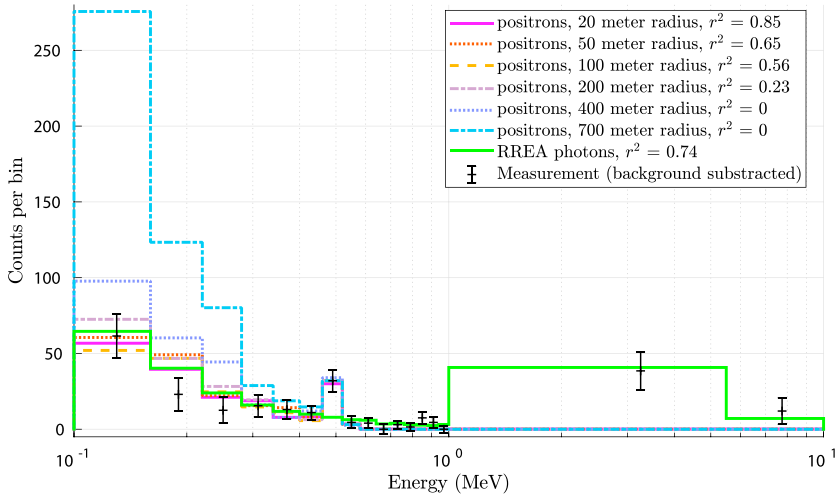

Figure 11. The results of the Geant4 simulations compared to the observed background subtracted spectrum. All positron spectra are normalized to have the same number of counts in 511 keV bin. The RREA photons spectrum is adjusted to the best fit to the measurement. The smallest radii of positron spheres 20, 50 and 100 m give the best match between simulation and observation. The spheres with 200 and 400 meter radii give the r-squared value of 0.23 and 0 respectively. The RREA photon model shows the r-squared value of 0.74 but is unable to reproduce the 511 keV bin.

4.1. Positron Annihilation Area

Simulating the spectral response to positron spheres of different sizes and fitting it to the measurement give an estimation of the size of the region where the annihilation is taking place (roughly following the analysis presented in Dwyer et al., 2015). Indeed, the larger the annihilation volume, the more Compton scattered photons will be detected. This results in a higher Compton component located roughly between 100 and 400 keV of the observed spectra.

In our simulations, the positrons are randomly sampled within spheres with several radii centered on the plane. They are generated in the air with density 3.035×10^{-4} g/cm^3 at 12-km altitude outside the aircraft. The results are shown in Figure 11. The photons are binned in 60-keV energy bins and plotted on logarithmic scale to better represent the low-energy Compton component. Photons from 1 to 10 MeV are binned into two 5-MeV bins for better visualization. As can be seen from the figure, the positron spheres of 20 to 40 m around the detector are already large enough to fit the size of the Compton continuum of the measured spectrum. The similarity between the simulation and the measurement can be quantified using the r-squared value. The 20-m radius model gives a value of $r^2 = 0.85$ excluding the last two bins above 1 MeV. Positron spheres with radii larger than 100 m result in a too large Compton continuum compared to the 511-keV bin and therefore fit less well ($r^2 = 0.65$ for 50 m and $r^2 = 0.56$ for 100 m). The r-squared value goes down to 0.23 for 200-m radius and falls down to zero for 400 m and above. This suggests that the positrons annihilate locally, perhaps at the aircraft itself.

In order to reproduce the detected 175 counts below 511 keV (background subtracted), it requires the annihilation of 1.6×10^8 positrons within a radius of 20 meters, or 5.9×10^8 within a radius of 50 meters, or 1.85×10^9

Table 2
Positron Annihilation Rate for Different Annihilation Radii

	Radius (m)	Rate (cm^3/s)
This work	20	0.5×10^{-2}
	50	1.1×10^{-3}
	100	0.5×10^{-3}
Dwyer et al. (2015)	450	$(5.8 \pm 2) \times 10^{-4}$
	900	$(2.2 \pm 0.7) \times 10^{-4}$
	2000	$(1.5 \pm 0.5) \times 10^{-4}$

within a radius of 100 meters. The positron annihilation rates obtained in this work and in Dwyer et al. (2015) are summarized in Table 2 for comparison.

4.2. Relativistic Runaway Electron Avalanche

Significant fraction of particles (1/3) in background subtracted spectrum have energy greater than 511 keV. Taking into account the decreasing absorption efficiency of the detector at high energy, the fraction is even larger. Therefore, the observed emission cannot be solely attributed to positron annihilation. In addition, the flux enhancement at moment A is superimposed on a gamma ray glow, and gamma ray glows were previously modeled by the RREA mechanism (Cramer et al., 2017; Kelley, 2014).

We tested the response of our Geant4 model to incident photons produced by RREA. If the RREA is fully developed, the emitted photon spectrum has approximately the analytical shape $f(\epsilon) = \exp(-\epsilon/7.3\ \mathrm{MeV})/\epsilon$, where ϵ is the photon energy. Photons sampled from this spectrum were propagated toward the aircraft, and the deposited energies on the detectors were recorded. Figure 11 shows the corresponding deposited energy spectrum (green line) compared with the measurements. It can be seen that the overall shape of the observed spectrum can be reproduced relatively well (r-squared value of 0.74), except the 511-keV bin. Therefore, the RREA hypothesis is unable to explain the observed 511-keV enhancement. Nevertheless, this is a simplified RREA simulation set-up and more advanced simulation should be performed following the full process of electron multiplication with an applied electric field. The simulation results are also sensitive to parameters like distance to the source, beaming, applied potential, and different seed electron spectra. In particular, it was showed by Cramer et al. (2014) that under some electric fields, RREA spectra can vary quite significantly from the standard exponential shape assumed here. A more detailed analysis of the RREA hypothesis is left for a future work.

5. Conclusions and Discussion

A sequence of 10 gamma ray enhancements was detected inside thundercloud, each lasted for about a second. Based upon the available data and analysis presented in this paper, we therefore conclude on following.

1. The charge buildup on the aircraft surface leads to negative discharges from static wicks.
2. The photon count rate increase is associated with these discharges. This conclusion is supported by direct optical observation and analysis of the ILDAS measurements.
3. The background subtracted spectrum of the photon emission contains 511-keV line that can only be prescribed to positron annihilation.
4. Most of the positron annihilation is taking place in direct vicinity of the aircraft. It is necessary to have at least 10^8 positrons annihilating to reproduce the measured flux.
5. A simplified RREA model cannot explain the observation.

Analysis of the E-field and H-field data allowed us to conclude that the discharges observed synchronously with the photon pulses are static discharges. The charge was accumulated on the aircraft surface either in collisions with neutral ice crystals or from charged particles of the cloud. The static discharges could induce the positron emission themselves or stimulate background positrons to annihilate.

None of the known high-energy atmospheric phenomena can explain the observation at current level of understanding. Some of the known emissions are too short (TGFs, lightning leader X-rays); some are too long or inconstant in appearance dynamic and spectrum (gamma ray glows). TGF afterglows are not consistent because the observed emission is clearly associated with periodic pulses of static discharges and not with a TGF. With the present data and available models of the high-energy atmospheric processes we cannot draw firm conclusions regarding the origin of the observed phenomenon. New airborne and spaceborne measurements are strongly desirable to advance our understanding. In the next years, two space missions specifically designed to study TGF will be in operation: the Atmosphere-Space Interaction Monitor (Neubert et al., 2006), and the Tool for the Analysis of Radiation from lightning and Sprites (Lefeuvre et al., 2009; Sarria et al., 2017).

We demonstrated that RREA mechanism is unlikely the source of the observed emission. Atmospheric discharges may possess another particle acceleration mechanism yet unknown to us. In addition to the new flight campaigns, we encourage other experimentalists to look for a long-lasting positron emission in high-voltage laboratories, especially after neutron generation events.

Appendix A: Geant4 Model

Since the detectors are located inside a massive aircraft (≈250 tons), most of what is produced outside has to interact with the air and the aircraft body before being detected. Furthermore, the detectors themselves have a response to the incident flux; in particular, they cannot detect any energy deposition above about 10 MeV. Therefore, to analyze the spectrum enhancement of this event, it is very important to model the whole system response. One way of handling this problem is to build a Geant4 model. Geant4 was developed by the European Organization for Nuclear Research CERN associated with a worldwide collaboration. It is used to simulate particle propagation through matter (Agostinelli et al., 2003; Allison et al., 2006), and it is an essential tool for simulating high-energy particle detectors. It is also capable of simulating the Relativistic Runaway Electron Avalanche mechanism, relativistic feedback (Skeltved et al., 2014), associated neutron emissions (Carlson et al., 2010), and electromagnetic particles propagation in air in high-energy atmospheric physics context (Rutjes et al., 2016).

The Geant4 mass model of the In-flight Lightning Damage Assessment System A340-600 aircraft has a size of about $75 \times 63 \times 17$ m^3 and is mostly composed of aluminum, in terms of mass. The main structure is made of a main tube of 2.8-m radius and 47-m length; several other tubes are added at the beginning and the end of the main tube to reproduce the cockpit, the tail, the wings, and the fins. We assumed that each of the tubes are made with a layer of aluminum with 4-mm thickness. The wings are approximated by several pieces of aluminum with reduced density in order to give them the correct mass and the overall shape very close to the real one. The inside of the aircraft is also modeled, including the floor, water tanks, racks, two computer stations, and chairs. The model of the two $LaBr_3$ detectors is very accurate and has been tested in a laboratory as described in Kochkin, Köhn, et al. (2016). The detectors are placed inside a polyvinyl chloride box. There is also a battery and a Sensor Assembly Electronics box located on the side of each detector. One detector is located near the center of the aircraft (X15) and the other in the rear part (X14), as shown in inset in Figure 7 and in Kochkin et al. (2015). When particle propagation is simulated, all energy deposited inside the $LaBr_3$ crystal are recorded. The detector resolution is assumed to be 4.5% full width at half maximum at 511 keV in order to produce the simulated spectra.

Acknowledgments
This work was supported by the European Research Council under the European Union's Seventh Framework Program(FP7/2007-2013)/ERC grant agreement 320839 and the Research Council of Norway under contracts 208028/F50 and 223252/F50 (CoE). Authors appreciate scientific discussions on different hypotheses with Nikolai Lehtinen, Andrey Mezentsev, and Georgi Genov from University of Bergen. The photon and E-field data used in this paper were uploaded in the supporting information and also available on request (pavlo.kochkin@uib.no).

References

Agostinelli, S., Allison, J., Amako, K., Apostolakis, J., Araujo, H., Arce, P., et al. (2003). GEANT4—A simulation toolkit. *Nuclear Instruments and Methods in Physics Research A*, *506*, 250–303. https://doi.org/10.1016/S0168-9002(03)01368-8

Allison, J., Amako, K., Apostolakis, J., Araujo, H., Dubois, P. A., Asai, M., et al. (2006). Geant4 developments and applications. *IEEE Transactions on Nuclear Science*, *53*, 270–278. https://doi.org/10.1109/TNS.2006.869826

Babich, L. P. (2006). Generation of neutrons in giant upward atmospheric discharges. *JETP Letters*, *84*(6), 285–288. https://doi.org/10.1134/S0021364006180020

Babich, L., & Bochkov, E. (2017). Numerical simulation of electric field enhancement at the contact of positive and negative streamers in relation to the problem of runaway electron generation in lightning and in long laboratory sparks. *Journal of Physics D: Applied Physics*, *50*(45), 455202.

Babich, L. P., Bochkov, E. I., Donskoi, E. N., & Kutsyk, I. M. (2010). Source of prolonged bursts of high-energy gamma rays detected in thunderstorm atmosphere in Japan at the coastal area of the sea of Japan and on high mountaintop. *Journal of Geophysical Research*, *115*, A09317. https://doi.org/10.1029/2009JA015017

Babich, L., & Loiko, T. (2009). Subnanosecond pulses of runaway electrons generated in atmosphere by high-voltage pulses of microsecond duration, Doklady Physics (Vol. 54, 479 pp.). Springer, SP MAIK Nauka/Interperiodica. https://doi.org/10.1134/S1028335809110019

Bowers, G. S., Smith, D. M., Martinez-McKinney, G., Kamogawa, M., Cummer, S., Dwyer, J., et al. (2017). Gamma-ray signatures of neutrons from a terrestrial gamma-ray flash. *Geophysical Research Letters*, *44*, 10,063–10,070. https://doi.org/10.1002/2017GL075071

Briggs, M., Fishman, G., Connaughton, V., Bhat, P., Paciesas, W., Preece, R., et al. (2010). First results on terrestrial gamma ray flashes from the fermi gamma-ray burst monitor. *Journal of Geophysical Research*, *115*, A07323. https://doi.org/10.1029/2009JA015242

Brunetti, M., Cecchini, S., Galli, M., Giovannini, G., & Pagliarin, A. (2000). Gamma-ray bursts of atmospheric origin in the MeV energy range. *Geophysical Research Letters*, *27*(11), 1599–1602.

Carlson, B. E., Lehtinen, N. G., & Inan, U. S. (2010). Neutron production in terrestrial gamma ray flashes. *Journal of Geophysical Research*, *115*, A00E19. https://doi.org/10.1029/2009JA014696

Carlson, B. E., Østgaard, N., Kochkin, P., Grondahl, Ø., Nisi, R., Weber, K., et al. (2015). Meter-scale spark X-ray spectrum statistics. *Journal of Geophysical Research: Atmospheres*, *120*, 11,191–11,202. https://doi.org/10.1002/2015JD023849

Chilingarian, A., Bostanjyan, N., & Vanyan, L. (2012). Neutron bursts associated with thunderstorms. *Physical review D*, *85*(8), 085017.

Chilingarian, A., Daryan, A., Arakelyan, K., Hovhannisyan, A., Mailyan, B., Melkumyan, L., et al. (2010). Ground-based observations of thunderstorm-correlated fluxes of high-energy electrons, gamma rays, and neutrons. *Physical Review D*, *82*(4), 043009.

Chilingarian, A., Hovsepyan, G., & Kozliner, L. (2013). Thunderstorm ground enhancements: Gamma ray differential energy spectra. *Physical Review D*, *88*(7), 073001.

Chilingarian, A., Vanyan, L., & Mailyan, B. (2013). Observation of thunderstorm ground enhancements with intense fluxes of high-energy electrons. *Astroparticle Physics*, *48*, 1–7.

Chubenko, A., Antonova, V., Kryukov, S. Y., Piskal, V., Ptitsyn, M., Shepetov, A., et al. (2000). Intensive X-ray emission bursts during thunderstorms. *Physics Letters A*, *275*(1), 90–100.

Connaughton, V., Briggs, M., Holzworth, R., Hutchins, M., Fishman, G., Wilson-Hodge, C., et al. (2010). Associations between fermi gamma-ray burst monitor terrestrial gamma ray flashes and sferics from the World Wide Lightning Location Network. *Journal of Geophysical Research*, *115*, A12307. https://doi.org/10.1029/2010JA015681

Connaughton, V., Briggs, M. S., Xiong, S., Dwyer, J. R., Hutchins, M. L., Grove, J. E., et al. (2013). Radio signals from electron beams in terrestrial gamma ray flashes. *Journal of Geophysical Research: Space Physics*, *118*, 2313–2320. https://doi.org/10.1029/2012JA018288

Cooray, V., Arevalo, L., Rahman, M., Dwyer, J., & Rassoul, H. (2009). On the possible origin of X-rays in long laboratory sparks. *Journal of Atmospheric and Solar-Terrestrial Physics*, *71*(17), 1890–1898.

Cramer, E. S., Dwyer, J. R., Arabshahi, S., Vodopiyanov, I. B., Liu, N., & Rassoul, H. K. (2014). An analytical approach for calculating energy spectra of relativistic runaway electron avalanches in air. *Journal of Geophysical Research: Space Physics*, *119*, 7794–7823. https://doi.org/10.1002/2014JA020265

Cramer, E. S., Mailyan, B. G., Celestin, S., & Dwyer, J. R. (2017). A simulation study on the electric field spectral dependence of thunderstorm ground enhancements and gamma ray glows. *Journal of Geophysical Research: Atmospheres*, *122*, 4763–4772. https://doi.org/10.1002/2016JD026422

Cummer, S. A., Lu, G., Briggs, M. S., Connaughton, V., Xiong, S., Fishman, G. J., & Dwyer, J. R. (2011). The lightning-TGF relationship on microsecond timescales. *Geophysical Research Letters*, *38*, L14810. https://doi.org/10.1029/2011GL048099

Cummer, S. A., Zhai, Y., Hu, W., Smith, D. M., Lopez, L. I., & Stanley, M. A. (2005). Measurements and implications of the relationship between lightning and terrestrial gamma ray flashes. *Geophysical Research Letters*, *32*, L08811. https://doi.org/10.1029/2005GL022778

de Boer, A. I., Bardet, S., Boissin, J., van Deursen, A. P. J., Flourens, F., & Herve, A. (2013). In-flight lightning damage assessment system (ILDAS): Further in-flight verification, with multi-sensor configuration.

de Boer, A. I., Bardet, M., Escure, C., Peres, G., Srithammavanh, V., Abboud, K., et al. (2011). In-flight lightning damage assessment system (ILDAS): Initial in-flight lightning tests and improvement of the numerical methods. In *ICOLSE 2011*, IEEE, Oxford, UK. September 2011.

de Boer, A. I., Flourens, F., Herve, A., Bardet, M., & Boissin, J. (2015). ILDAS2: From the laboratory to operations-benefits and performance of the in-flight lightning damage assessment system in support of flight test campaigns. In *IET Conference Proceedings*, The Institution of Engineering & Technology.

Dwyer, J. R., Rassoul, H. K., Al-Dayeh, M., Caraway, L., Chrest, A., Wright, B., et al. (2005). X-ray bursts associated with leader steps in cloud-to-ground lightning. *Geophysical Research Letters*, *32*, L01803. https://doi.org/10.1029/2004GL021782

Dwyer, J., Rassoul, H., Al-Dayeh, M., Caraway, L., Wright, B., Chrest, A., et al. (2004). Measurements of X-ray emission from rocket-triggered lightning. *Geophysical Research Letters*, *31*, L05118. https://doi.org/10.1029/2003GL018770

Dwyer, J. R., Rassoul, H. K., Saleh, Z., Uman, M. A., Jerauld, J., & Plumer, J. A. (2005). X-ray bursts produced by laboratory sparks in air. *Geophysical Research Letters*, *32*, L20809. https://doi.org/10.1029/2005GL024027

Dwyer, J. R., Saleh, Z., Rassoul, H. K., Concha, D., Rahman, M., Cooray, V., et al. (2008). A study of X-ray emission from laboratory sparks in air at atmospheric pressure. *Journal of Geophysical Research*, *113*, D23207. https://doi.org/10.1029/2008JD010315

Dwyer, J., Schaal, M., Cramer, E., Arabshahi, S., Liu, N., Rassoul, H., et al. (2012). Observation of a gamma-ray flash at ground level in association with a cloud-to-ground lightning return stroke. *Journal of Geophysical Research*, *117*, A10303. https://doi.org/10.1029/2012JA017810

Dwyer, J. R., Schaal, M., Rassoul, H. K., Uman, M. A., Jordan, D. M., & Hill, D. (2011). High-speed X-ray images of triggered lightning dart leaders. *Journal of Geophysical Research*, *116*, D20208. https://doi.org/10.1029/2011JD015973

Dwyer, J. R., & Smith, D. M. (2005). A comparison between Monte Carlo simulations of runaway breakdown and terrestrial gamma-ray flash observations. *Geophysical Research Letters*, *32*, L22804. https://doi.org/10.1029/2005GL023848

Dwyer, J. R., Smith, D. M., & Cummer, S. A. (2012). High-energy atmospheric physics: Terrestrial gamma-ray flashes and related phenomena. *Space Science Reviews*, *173*(1-4), 133–196.

Dwyer, J. R., Smith, D. M., Hazelton, B. J., Grefenstette, B. W., Kelley, N. A., Lowell, A. W., et al. (2015). Positron clouds within thunderstorms. *Journal of Plasma Physics*, *81*(04), 475810405.

Dwyer, J. R., Uman, M. A., Rassoul, H. K., Al-Dayeh, M., Caraway, L., Jerauld, J., et al. (2003). Energetic radiation produced during rocket-triggered lightning. *Science*, *299*(5607), 694–697.

Eack, K. B., Beasley, W. H., Rust, W. D., Marshall, T. C., & Stolzenburg, M. (1996a). Initial results from simultaneous observation of X-rays and electric fields in a thunderstorm. *Journal of Geophysical Research*, *101*(D23), 29,637–29,640.

Eack, K. B., Beasley, W. H., Rust, W. D., Marshall, T. C., & Stolzenburg, M. (1996b). X-ray pulses observed above a mesoscale convective system. *Geophysical Research Letters*, *23*(21), 2915–2918.

Eack, K. B., Suszcynsky, D. M., Beasley, W. H., Roussel-Dupre, R., & Symbalisty, E. (2000). Gamma-ray emissions observed in a thunderstorm anvil. *Geophysical Research Letters*, *27*(2), 185–188.

Fishman, G. J., Bhat, P., Mallozzi, R., Horack, J., Koshut, T., Kouveliotou, C., et al. (1994). Discovery of intense gamma-ray flashes of atmospheric origin. *Science-AAAS-Weekly Paper Edition-including Guide to Scientific Information*, *264*(5163), 1313–1316.

Gjesteland, T., Østgaard, N., Bitzer, P., & Christian, H. J. (2017). On the timing between terrestrial gamma ray flashes, radio atmospherics and optical lightning emission. *Journal of Geophysical Research: Space Physics*, *122*, 7734–7741. https://doi.org/10.1002/2017JA024285

Gjesteland, T., Østgaard, N., Collier, A., Carlson, B., Cohen, M., & Lehtinen, N. (2011). Confining the angular distribution of terrestrial gamma ray flash emission. *Journal of Geophysical Research*, *116*, A11313. https://doi.org/10.1029/2011JA016716

Gjesteland, T., Østgaard, N., Collier, A., Carlson, B., Eyles, C., & Smith, D. (2012). A new method reveals more TGFs in the rhessi data. *Geophysical Research Letters*, *39*, L05102. https://doi.org/10.1029/2012GL050899

Gjesteland, T., Østgaard, N., Connell, P., Stadsnes, J., & Fishman, G. (2010). Effects of dead time losses on terrestrial gamma ray flash measurements with the burst and transient source experiment. *Journal of Geophysical Research*, *115*, A00E21. https://doi.org/10.1029/2009JA014578

Grefenstette, B. W., Smith, D. M., Dwyer, J. R., & Fishman, G. J. (2008). Time evolution of terrestrial gamma ray flashes. *Geophysical Research Letters*, *35*, L06802. https://doi.org/10.1029/2007GL032922

Gurevich, A., Antonova, V., Chubenko, A., Karashtin, A., Mitko, G., Ptitsyn, M., et al. (2012). Strong flux of low-energy neutrons produced by thunderstorms. *Physical Review Letters*, *108*(12), 125001.

Gurevich, A., Milikh, G., & Roussel-Dupre, R. (1992). Runaway electron mechanism of air breakdown and preconditioning during a thunderstorm. *Physics Letters A*, *165*(5-6), 463–468.

Hare, B., Uman, M., Dwyer, J., Jordan, D., Biggerstaff, M., Caicedo, J., et al. (2016). Ground-level observation of a terrestrial gamma ray flash initiated by a triggered lightning. *Journal of Geophysical Research: Atmospheres*, *121*, 6511–6533. https://doi.org/10.1002/2015JD02442610

Hill, J. D. (2012). *The mechanisms of lightning leader propagation and ground attachment*. Gainesville, Florida: University of Florida.

Hill, J. D., Uman, M. A., Jordan, D. M., Dwyer, J. R., & Rassoul, H. (2012). "chaotic" dart leaders in triggered lightning: Electric fields, X-rays, and source locations. *Journal of Geophysical Research*, *117*, D03118. https://doi.org/10.1029/2011JD016737

HIMAWARI-8 (2017). Cooperative institute for meteorological satellite studies, data retrieved October, 24 2017 from http://tropic.ssec.wisc.edu/archive/

Howard, J., Uman, M. A., Biagi, C., Hill, D., Jerauld, J., Rakov, V. A., et al. (2010). RF and X-ray source locations during the lightning attachment process. *Journal of Geophysical Research*, *115*, D06204. https://doi.org/10.1029/2009JD012055

Howard, J., Uman, M. A., Dwyer, J. R., Hill, D., Biagi, C., Saleh, Z., et al. (2008). Co-location of lightning leader X-ray and electric field change sources. *Geophysical Research Letters*, *35*, L13817. https://doi.org/10.1029/2008GL034134

Ihaddadene, M. A., & Celestin, S. (2015). Increase of the electric field in head-on collisions between negative and positive streamers. *Geophysical Research Letters*, *42*, 5644–5651. https://doi.org/10.1002/2015GL064623

Illingworth, A., & Marsh, S. (1986). Static charging of aircraft by collisions with ice crystals. *Revue De Physique Appliquee*, *21*(12), 803–808.

Kelley, N. (2014). Long duration gamma-ray emission from thunderclouds (PhD Thesis), University of, California, Santa Cruz.

Kelley, N. A., Smith, D. M., Dwyer, J. R., Splitt, M., Lazarus, S., Martinez-McKinney, F., et al. (2015). Relativistic electron avalanches as a thunderstorm discharge competing with lightning. *Nature Communications*, *6*, 7845.

Kochkin, P. (2014). Understanding lightning: Experiments on meter long discharges and their X-rays (PhD Dissertation), Eindhoven University of Technology.

Kochkin, P., Köhn, C., Ebert, U., & van Deursen, A. P. J. (2016). Analyzing X-ray emissions from meter-scale negative discharges in ambient air. *Plasma Sources Science and Technology*, *25*, 044002.

Kochkin, P., Lehtinen, N., van Deursen, A. P. J., & Østgaard, N. (2016). Pilot system development in metre-scale laboratory discharge. *Journal of Physics D: Applied Physics*, *49*(42), 425203.

Kochkin, P. O., Nguyen, C. V., van Deursen, A. P. J., & Ebert, U. (2012). Experimental study of hard X-rays emitted from metre-scale positive discharges in air. *Journal of Physics D: Applied Physics*, *45*(42), 425202.

Kochkin, P., van Deursen, A., de Boer, A., Bardet, M., & Boissin, J.-F. (2015). Journal of Physics D: Applied Physics, *48*(42), 425202.

Kochkin, P. O., van Deursen, A. P. J., & Ebert, U. (2014a). Experimental study of the spatio-temporal development of metre-scale negative discharge in air. *Journal of Physics D: Applied Physics*, *47*(14), 145203.

Kochkin, P. O., van Deursen, A. P. J., & Ebert, U. (2014b). Experimental study on hard X-rays emitted from metre-scale negative discharges in air. *Journal of Physics D: Applied Physics*, *48*(2), 025205.

Kochkin, P., van Deursen, A. P. J., Marisaldi, M., Ursi, A., de Boer, A. I., Bardet, M., et al. (2017). In-flight observation of gamma-ray glows by ILDAS. *Journal of Geophysical Research: Atmospheres*, *122*, 12,801–12,811. https://doi.org/10.1002/2017JD027405

Köhn, C., Chanrion, O., & Neubert, T. (2017). Electron acceleration during streamer collisions in air. *Geophysical Research Letters*, *44*, 2604–2613. https://doi.org/1002/2016GL072216

Kuroda, Y., Oguri, S., Kato, Y., Nakata, R., Inoue, Y., Ito, C., & Minowa, M. (2016). Observation of gamma ray bursts at ground level under the thunderclouds. *Physics Letters B*, *758*, 286–291.

Lalande, P., Bondiou-Clergerie, A., & Laroche, P. (1999). Analysis of available in-flight measurements of lightning strikes to aircraft (Tech. Rep.). SAE Technical Paper. https://doi.org/10.4271/1999-01-2397

Laroche, P., Blanchet, P., Delannoy, A., & Issac, F. (2012). Experimental studies of lightning strikes to aircraft, AerospaceLab, (5), p–1.

Lefeuvre, F., Blanc, E., & Pinçon, J. L. (2009). TARANIS — A satellite project dedicated to the physics of TLEs and TGFs. In *American Institute of Physics Conference Series*, *1118*, pp. 3–7. https://doi.org/10.1063/1.3137711

Mallick, S., Rakov, V., & Dwyer, J. (2012). A study of X-ray emissions from thunderstorms with emphasis on subsequent strokes in natural lightning. *Journal of Geophysical Research*, *117*, D16107. https://doi.org/10.1029/2012JD017555

March, V., & Montanyà, J. (2010). Influence of the voltage-time derivative in X-ray emission from laboratory sparks. *Geophysical Research Letters*, *37*, L19801. https://doi.org/10.1029/2010GL044543

March, V., & Montanyà, J. (2011). X-rays from laboratory sparks in air: The role of the cathode in the production of runaway electrons. *Geophysical Research Letters*, *38*, L04803.

March, V., Montanya, J., Romero, D., Solà, G., & Van der Welde, O. (2012). X-rays from laboratory sparks in air: The relationship between runaway electrons and the electric field. In *Lightning Protection (ICLP), 2012 International Conference on*, IEEE, pp. 1–7.

Marisaldi, M., Argan, A., Trois, A., Giuliani, A., Tavani, M., Labanti, C., et al. (2010). Gamma-ray localization of terrestrial gamma-ray flashes. *Physical Review Letters*, *105*(12), 128501.

Marisaldi, M., Fuschino, F., Labanti, C., Galli, M., Longo, F., Del Monte, E., et al. (2010). Detection of terrestrial gamma ray flashes up to 40 MeV by the AGILE satellite. *Journal of Geophysical Research*, *115*, A3. https://doi.org/10.1029/2009JA014502

Marisaldi, M., Fuschino, F., Tavani, M., Dietrich, S., Price, C., Galli, M., et al. (2014). Properties of terrestrial gamma ray flashes detected by AGILE MCAL below 30 MeV. *Journal of Geophysical Research: Space Physics*, *119*, 1337–1355. https://doi.org/10.1002/2013JA019301

Mazur, V., Fisher, B., & Gerlach, J. (1984). Lightning strikes to an airplane in a thunderstorm. *Journal of Aircraft*, *21*(8), 607–611.

Mazur, V., & Ruhnke, L. H. (1993). Common physical processes in natural and artificially triggered lightning. *Journal of Geophysical Research*, *98*(D7), 12,913–12,930.

McCarthy, M., & Parks, G. (1985). Further observations of X-rays inside thunderstorms. *Geophysical research letters*, *12*(6), 393–396.

McCarthy, M. P., & Parks, G. K. (1992). On the modulation of X ray fluxes in thunderstorms. *Journal of Geophysical Research*, *97*(D5), 5857–5864.

Mezentsev, A., Lehtinen, N., Ostgaard, N., Perez-Invernon, J., & Cummer, S. (2017). Spectral characteristics of VLF sferics associated with TGFs. In *EGU General Assembly Conference Abstracts*, *19*, pp. 11285.

Montanyà, J., Van der Velde, O., March, V., Romero, D., Solà, G., & Pineda, N. (2012). High-speed video of lightning and X-ray pulses during the 2009–2010 observation campaigns in northeastern Spain. *Atmospheric research*, *117*, 91–98.

Moore, C. B., Eack, K. B., Aulich, G. D., & Rison, W. (2001). Energetic radiation associated with lightning stepped-leaders. *Geophysical Research Letters*, *28*(11), 2141–2144.

Moreau, J.-P., Alliot, J.-C., & Mazur, V. (1992). Aircraft lightning initiation and interception from in situ electric measurements and fast video observations. *Journal of Geophysical Research*, *97*(D14), 15,903–15,912.

Muehleisen, R. (1980). Phenomenology of lightning/aircraft interaction. In AGARD Atmospheric Elec.-Aircraft Interaction 6 p (SEE N80-31743 22-33).

Neubert, T., Kuvvetli, I., Budtz-Jørgensen, C., Østgaard, N., Reglero, V., & Arnold, N. (2006). The atmosphere-space interactions monitor (ASIM) for the international space station. In N. Gopalswamy & A. Bhattacharyya (Eds.), *Proceedings of the ILWS Workshop* (pp. 448).

Nguyen, C. V., van Deursen, A. P. J., & Ebert, U. (2008). Multiple X-ray bursts from long discharges in air. *Journal of Physics D: Applied Physics*, *41*(23), 234012.

Nguyen, C., Van Deursen, A. P. J., Van Heesch, E., Winands, G., & Pemen, A. (2009). X-ray emission in streamer-corona plasma. *Journal of Physics D: Applied Physics*, *43*(2), 025202.

Østgaard, N., Carlson, B., Nisi, R., Gjesteland, T., Grøndahl, Ø., Skeltved, A., et al. (2016). Relativistic electrons from sparks in the laboratory. *Journal of Geophysical Research: Atmospheres*, *121*, 2939–2954. https://doi.org/10.1002/2015JD024394

Østgaard, N., Gjesteland, T., Carlson, B., Collier, A., Cummer, S., Lu, G., & Christian, H. (2013). Simultaneous observations of optical lightning and terrestrial gamma ray flash from space. *Geophysical Research Letters*, *40*, 2423–2426. https://doi.org/10.1002/grl.50466

Østgaard, N., Gjesteland, T., Hansen, R., Collier, A., & Carlson, B. (2012). The true fluence distribution of terrestrial gamma flashes at satellite altitude. *Journal of Geophysical Research*, *117*, A03327. https://doi.org/10.1029/2011JA017365

Østgaard, N., Gjesteland, T., Stadsnes, J., Connell, P., & Carlson, B. (2008). Production altitude and time delays of the terrestrial gamma flashes: Revisiting the burst and transient source experiment spectra. *Journal of Geophysical Research*, *113*, A02307. https://doi.org/10.1029/2007JA012618

Parks, G., Mauk, B., Spiger, R., & Chin, J. (1981). X-ray enhancements detected during thunderstorm and lightning activities. *Geophysical Research Letters*, *8*(11), 1176–1179.

Rahman, M., Cooray, V., Ahmad, N. A., Nyberg, J., Rakov, V. A., & Sharma, S. (2008). X rays from 80-cm long sparks in air. *Geophysical Research Letters*, *35*, L06805. https://doi.org/10.1029/2007GL032678

Rep'ev, A., Repin, P., & Danchenko, E. (2008). Structure of the glow of a nanosecond diffuse discharge in a strongly nonuniform electric field. *Technical Physics*, *53*(7), 858–865.

Rodger, C., Brundell, J., Dowden, R., & Thomson, N. (2004). Location accuracy of long distance VLF lightning location network. *Annales Geophysicae*, *22*, 747–758.

Rozsa, C., Menge, P., & Mayhugh, M. (2009). Brillance scintillators performance summary, Scintillation Products Technical Note, Saint-Gobain Crystals. http://www.detectors.saint-gobain.com

Rutjes, C., Diniz, G., Ferreira, I. S., & Ebert, U. (2017). Tgf afterglows: A new radiation mechanism from thunderstorms. *Geophysical Research Letters*, *44*, 10,702–10,712. https://doi.org/10.1002/2017GL075552

Rutjes, C., Sarria, D., Skeltved, A. B., Luque, A., Diniz, G., Østgaard, N., & Ebert, U. (2016). Evaluation of Monte Carlo tools for high energy atmospheric physics. *Geoscientific Model Development*, *9*(11), 3961–3974. https://doi.org/10.5194/gmd-9-3961-2016

Saleh, Z., Dwyer, J., Howard, J., Uman, M., Bakhtiari, M., Concha, D., et al. (2009). Properties of the X-ray emission from rocket-triggered lightning as measured by the Thunderstorm Energetic Radiation Array (TERA). *Journal of Geophysical Research*, *114*, D17210. https://doi.org/10.1029/2008JD011618

Sarria, D., Lebrun, F., Blelly, P.-L., Chipaux, R., Laurent, P., Sauvaud, J.-A., et al. (2017). TARANIS XGRE and IDEE detection capability of terrestrial gamma-ray flashes and associated electron beams. *Geoscientific Instrumentation, Methods and Data Systems*, *6*(2), 239–256. https://doi.org/10.5194/gi-6-239-2017

Schaal, M., Dwyer, J. R., Arabshahi, S., Cramer, E. S., Lucia, R., Liu, N., et al. (2014). The structure of X-ray emissions from triggered lightning leaders measured by a pinhole-type X-ray camera. *Journal of Geophysical Research: Atmospheres*, *119*, 982–1002. https://doi.org/10.1002/2013JD020266

Schaal, M., Dwyer, J. R., Rassoul, H. K., Hill, J. D., Jordan, D. M., & Uman, M. A. (2013). The angular distribution of energetic electron and X-ray emissions from triggered lightning leaders. *Journal of Geophysical Research: Atmospheres*, *118*, 11,712–11,726. https://doi.org/10.1002/2013JD019619

Schaal, M., Dwyer, J., Saleh, Z., Rassoul, H., Hill, J., Jordan, D., & Uman, M. (2012). Spatial and energy distributions of X-ray emissions from leaders in natural and rocket triggered lightning. *Journal of Geophysical Research*, *117*, D15201. https://doi.org/10.1029/2012JD017897

Skeltved, A. B., Ostgaard, N., Carlson, B., Gjesteland, T., & Celestin, S. (2014). Modeling the relativistic runaway electron avalanche and the feedback mechanism with GEANT4. *Journal of Geophysical Research: Space Physics*, *119*, 9174–9191. https://doi.org/10.1002/2014JA020504

Smith, D., Dwyer, J., Hazelton, B., Grefenstette, B., Martinez-McKinney, G., Zhang, Z., et al. (2011a). A terrestrial gamma ray flash observed from an aircraft. *Journal of Geophysical Research*, *116*, D20124. https://doi.org/10.1029/2011JD016252

Smith, D., Dwyer, J., Hazelton, B., Grefenstette, B., Martinez-McKinney, G., Zhang, Z., et al. (2011b). The rarity of terrestrial gamma-ray flashes. *Geophysical Research Letters*, *38*, L08807. https://doi.org/10.1002/2016JD025395

Smith, D. M., Lopez, L. I., Lin, R. P., & Barrington-Leigh, C. P. (2005). Terrestrial gamma-ray flashes observed up to 20 MeV. *Science*, *307*(5712), 1085–1088.

Stelmashuk, V., van Deursen, A. P. J., & Webster, M. (2008). Sensors for in-flight lightning detection on aircraft. In *2008 International Symposium on Electromagnetic Compatibility-EMC Europe*, IEEE, pp. 1–5.

Stelmashuk, V., van Deursen, A. P. J., & Zwemmer, R. (2007). Sensor development for the ILDAS project. In *EMC Europe Workshop, Paris*.

Tanner, R., & Nanevicz, J. (1961). Precipitation charging and corona-generated interference in aircraft (Tech. Rep.). MENLO PARK CA: STANFORD RESEARCH INST.

Tavani, M., Marisaldi, M., Labanti, C., Fuschino, F., Argan, A., Trois, A., et al. (2011). Terrestrial gamma-ray flashes as powerful particle accelerators. *Physical Review Letters*, *106*(1), 018501.

Teruaki, E., Wada, Y., Furuta, Y., Nakazawa, K., Yuasa, T., Okuda, K., et al. (2017). Photonuclear reactions triggered by lightning discharge. *Nature*, *551*(481). https://doi.org/10.1038/nature24630

Torii, T., Sugita, T., Tanabe, S., Kimura, Y., Kamogawa, M., Yajima, K., & Yasuda, H. (2009). Gradual increase of energetic radiation associated with thunderstorm activity at the top of Mt. Fuji. *Geophysical Research Letters*, *36*, L13804. https://doi.org/10.1029/2008GL037105

Torii, T., Takeishi, M., & Hosono, T. (2002). Observation of gamma-ray dose increase associated with winter thunderstorm and lightning activity. *Journal of Geophysical Research*, *107*(D17), 4324. https://doi.org/10.1029/2001JD000938

Tsuchiya, H., Enoto, T., Yamada, S., Yuasa, T., Kawaharada, M., Kitaguchi, T., et al. (2007). Detection of high-energy gamma rays from winter thunderclouds. *Physical Review Letters*, *99*(16), 165002.

Tsuchiya, H., Hibino, K., Kawata, K., Hotta, N., Tateyama, N., Ohnishi, M., et al. (2012). Observation of thundercloud-related gamma rays and neutrons in Tibet. *Physical Review D*, *85*(9), 092006.

van Deursen, A. P. J. (2011). Inductive sensor for lightning current measurement, fitted in aircraft windows—Part II: Measurements on an a320 aircraft. *IEEE Sensors Journal*, *11*(1), 205–209.

van Deursen, A. P. J., & Stelmashuk, V. (2011). Inductive sensor for lightning current measurement, fitted in aircraft windows—Part I: Analysis for a circular window. *IEEE Sensors Journal*, *11*(1), 199.

Yoshida, S., Morimoto, T., Ushio, T., Kawasaki, Z.-I., Torii, T., Wang, D., et al. (2008). High energy photon and electron bursts associated with upward lightning strokes. *Geophysical Research Letters*, *35*, L10804. https://doi.org/10.1029/2007GL032438

Zwemmer, R., Bardet, M., de Boer, A., Hardwick, J., Hawkins, K., Morgan, D., et al. (2009). In-flight lightning damage assessment system (ILDAS); results of the concept prototype tests. In *Proc. Int. Conf. ICOLSE*.